Nuclear-relaxed elastic and piezoelectric constants of materials: Computational aspects of two quantum-mechanical approaches

Nuclear-relaxed Elastic and Piezoelectric Constants of Materials: Computational Aspects of Two Quantum-mechanical Approaches

A. Erba,[1,*] D. Caglioti,[1] C. M. Zicovich-Wilson,[2] and R. Dovesi[1]

[1] *Dipartimento di Chimica, Università di Torino and NIS, Nanostructured Interfaces and Surfaces, Centre of Excellence, Via Giuria 5, 10125 Torino, Italy*

[2] *Centro de Investigación en Ciencias-(IICBA), Universidad Autónoma del Estado de Morelos, Av. Universidad, 1001, Col. Chamilpa, 62209 Cuernavaca, Morelos, Mexico*

(Dated: November 11, 2016)

Two alternative approaches for the quantum-mechanical calculation of the nuclear-relaxation term of elastic and piezoelectric tensors of crystalline materials are illustrated and their computational aspects discussed: i) a numerical approach based on the geometry optimization of atomic positions at strained lattice configurations and ii) a quasi-analytical approach based on the evaluation of the force- and displacement-response internal-strain tensors as combined with the interatomic force-constant matrix. The two schemes are compared both as regards their computational accuracy and performance. The latter approach, not being affected by the many numerical parameters and procedures of a typical quasi-Newton geometry optimizer, constitutes a more reliable and robust mean to the evaluation of such properties, at a reduced computational cost for most crystalline systems.

I. INTRODUCTION

First-principle calculations based on the density functional theory (DFT) do constitute an effective mean to the accurate evaluation of several strain-related properties of solids: third-rank direct and converse piezoelectric, fourth-rank elastic stiffness and compliance, fourth-rank photo-elastic and piezo-optic tensors.[1–19] The quantum-mechanical determination of such high-order tensorial properties involves the evaluation of high-order total energy derivatives with respect to three main kinds of perturbations: atomic displacements, homogeneous strains and electric fields.[20,21] It follows that the determination of all components of any of these tensors represents a computationally demanding task, at least in two respects: i) large number of required fundamental calculations (for instance, use is commonly made of external programs and scripts that run many independent calculations and then collect and analyze computed energies or energy gradients for the calculation of the elastic tensor, in combination with popular plane-wave programs);[13,22] ii) large fraction of "numerical" steps involved in standard formulations (e.g. second-energy derivatives with respect to either atomic displacements or lattice strains are commonly obtained as finite differences, and the polarization in solids is often obtained numerically from a Berry-phase approach).[10,12–14] Furthermore, numerical geometry optimizations of atomic coordinates at strained lattice configurations are usually performed in order to account for nuclear-relaxation contributions, which are known to be dominant with respect to purely electronic contributions in most cases.[23,24]

As regards the two main sources of computational complexity briefly addressed above, they can be progressively overcome by following two general prescriptions: i) by devising automated algorithms, capable of managing the large number of required calculations and reducing (or even completely eliminating) any explicit intermediate action from the user; ii) by reducing the weight of the involved "numerical" steps in favor of more "analytical" procedures. In the implementation into the CRYSTAL program of strain-related tensorial properties of solids, we have tried to follow these two prescriptions during the last ten years or so. Let us briefly review the various developments made in this respect:

- With the CRYSTAL03 and CRYSTAL06 versions of the program, elastic and piezoelectric tensors could be computed by running several individual calculations and then by merging them via external scripts. Elastic constants were computed as numerical energy second-derivatives with respect to lattice strains, piezoelectric constants were computed as numerical finite differences of numerically computed Berry phases, and numerical geometry optimizations were used for the nuclear relaxation contribution of both tensors.[25–27]

- In the CRYSTAL09 version of the program, a fully-automated implementation of the elastic tensor was devised (i.e. requiring a single run for the whole tensor), where elastic constants were obtained as numerical derivatives of analytical lattice gradients.[10,11,28,29]

- In the CRYSTAL14 version, a fully-automated algorithm was implemented for computing the direct piezoelectric tensor via the Berry-phase approach and (through the simultaneous evaluation of the elastic tensor) the converse piezoelectric tensor as well. The calculation of elastic and piezoelectric tensors was also generalized to low-dimensional 1D and 2D systems.[4,30]

- A fully-automated scheme was also devised and implemented for the evaluation of the fourth-rank

photo-elastic tensor, where elasto-optic constants were obtained as numerical first-derivatives with respect to the strain of analytical dielectric tensor components, as computed through a Coupled-Perturbed-Hartree-Fock/Kohn-Sham (CPHF/KS) approach.[17]

- In a developmental version of the program (to be soon released as CRYSTAL17), a fully-automated scheme has been implemented for the analytical calculation of the direct piezoelectric tensor though the CPHF/KS approach.[31]

- A fully-automated procedure, based on the analytical evaluation of the stress tensor,[32] has been developed for the determination of pressure-dependent elastic constants.[33]

- A fully-automated algorithm has been devised (which requires the simultaneous evaluation of the fourth-rank elastic and photo-elastic tensors) for the calculation of the fourth-rank piezo-optic tensor of crystals.[18,19]

- A fully-automated algorithm, with a full exploitation of all translational and point symmetry features, has also been implemented for the evaluation of nuclear-relaxed elastic and piezoelectric constants of crystalline materials, where the "quasi-analytical" formulation in terms of the internal-strain tensor is used instead of the standard "numerical" approach requiring geometry optimizations at strained lattice configurations.[34]

In this paper, in particular, we shall discuss the main computational implications of the last (and most recent) development reported in the list above. That is, the new, quasi-analytical, formulation in terms of the internal-strain tensor of energy second-derivatives with respect to atomic displacements and lattice deformations, as combined with the interatomic force-constant Hessian matrix, is compared with the previous approach involving the numerical relaxation of atomic positions upon strain. The comparison is performed in terms of both accuracy and computational performance. Two systems will be analyzed into detail, which, belonging to non-centro-symmetric space groups, exhibit both an elastic and a piezoelectric response: hexagonal zinc oxide (ZnO), and trigonal α-quartz. These two systems have already served as test cases in a couple of recent studies on strain-related properties and therefore constitute an optimal benchmark.[31,34] Furthermore, in order to investigate whether or not the computational performance advantages of one scheme with respect to the other could depend on the richness of the point-symmetry features of the system under investigation, seven crystals shall be considered, belonging to the seven possible crystalline systems (from cubic to triclinic).

The structure of the paper is as follows: Section II is devoted to the formal and methodological description of the "geometry optimizer" (GO) and "internal-strain tensor" (IST) approaches for the quantum-mechanical evaluation of nuclear-relaxed elastic and piezoelectric constants of materials; the two approaches are compared in terms of both numerical accuracy and computational performance in Section III; conclusions are drawn in Section IV.

II. FORMAL AND COMPUTATIONAL ASPECTS

Second-order elastic constants of a crystal at its equilibrium volume V_0 are expressed as second energy derivatives with respect to pairs of homogeneous strains:

$$C_{vw} = \frac{1}{V_0} \left. \frac{\partial^2 E}{\partial \eta_v \partial \eta_w} \right|_{\mathcal{E}} = \frac{1}{V_0} \left. \frac{\partial g_v}{\partial \eta_w} \right|_{\mathcal{E}} , \qquad (1)$$

where the derivatives are taken at constant electric field $\mathcal{E}$ (to ensure formal compatibility with the piezoelectric constants to be defined below), the symmetric second-rank pure strain tensor $\boldsymbol{\eta}$ is represented by adopting Voigt's notation according to which $v = 1 \equiv xx$, $v = 2 \equiv yy$, $v = 3 \equiv zz$, $v = 4 \equiv yz$, $v = 5 \equiv xz$, and $v = 6 \equiv xy$,[35] and where we have introduced the lattice strain energy gradient $g_v = \partial E / \partial \eta_v |_{\mathcal{E}}$. In the CRYSTAL program, strain energy gradients g_v are computed analytically[28,29] and the second energy derivatives in Eq. (1) can be evaluated as their numerical finite differences (via a double-sided formula):

$$C_{vw} = \frac{1}{V_0} \left[g_v|_{\eta_w = \overline{\eta}} - g_v|_{\eta_w = -\overline{\eta}} \right] / 2\overline{\eta} , \qquad (2)$$

where $\overline{\eta}$ is the amplitude of the applied strain, which has been optimized to the default value of 1%.[10,11]

First-order direct piezoelectric constants are expressed as second energy derivatives with respect to electric field Cartesian components and lattice strains:

$$e_{kv} = \frac{1}{V_0} \frac{\partial^2 E}{\partial \mathcal{E}_k \partial \eta_v} \cong \frac{\partial P_k}{\partial \eta_v} , \qquad (3)$$

where P_k is the k-th Cartesian component of the polarization vector. For a more accurate account of the subtleties related to the distinction between "proper" and "improper" piezoelectric coefficients (evaluated/measured in terms of a voltage or electric field, respectively), the reader may refer to Refs. 2,20,31,36–38. A fully-analytical approach has recently been devised for the direct evaluation of the electronic term of the second-derivatives in Eq. (3), via a CPHF/KS approach.[31] The most popular technique for evaluating piezoelectric constants still remains the numerical Berry phase approach, within the modern theory of polarization of solids, though,[1–3] according to which constants e_{kv} are obtained from polarization (i.e. Berry phase) finite differences at strained configurations:

$$e_{kv} = \left[P_k|_{\eta_v = \overline{\eta}} - P_k|_{\eta_v = -\overline{\eta}} \right] / 2\overline{\eta} , \qquad (4)$$

where a double-sided formula with a strain amplitude $\overline{\eta}$ of 1.5% is used as a default in the implementation into the CRYSTAL program.

Strain-induced response properties of solids can be formally decomposed into a purely electronic "clamped-nuclei" term and a nuclear-relaxation term due to the rearrangement of atomic positions upon strain. In Sections II A and II B we shall now introduce two alternative strategies for the evaluation of the nuclear-relaxation term.

A. The Geometry Optimizer Approach

Total (i.e. electronic plus nuclear-relaxation) or electronic only elastic and piezoelectric constants can be obtained by evaluating the strain derivatives in Eqs. (1) and (3) by allowing or not atomic positions u to relax at strained lattice configurations, respectively. It follows that the nuclear-relaxation contribution can be obtained as difference between total and electronic "clamped-nuclei" values:

$$C_{vw}^{\rm nuc} = \frac{1}{V_0}\left[\left.\frac{\partial g_v}{\partial \eta_w}\right|_{\mathcal{E}} - \left.\frac{\partial g_v}{\partial \eta_w}\right|_{\mathcal{E},u}\right] \quad (5)$$

$$e_{kv}^{\rm nuc} = \left[\frac{\partial P_k}{\partial \eta_v} - \left.\frac{\partial P_k}{\partial \eta_v}\right|_{u}\right] . \quad (6)$$

A schematic representation of the fully-automated algorithm (i.e. requiring a single run calculation) implemented in the CRYSTAL program for computing elastic constants via the geometry optimizer approach is sketched in Figure 1.

A quasi-Newton scheme for energy minimization is implemented in the CRYSTAL program,[39] which is based on the calculation of analytical energy gradients at each optimization step.[28,29,40,41] The initial guess for the Hessian matrix of energy second derivatives is obtained through a classical force-field model as proposed by Schlegel.[42] During the optimization, the Hessian is updated from the gradients by means of the Broyden-Fletcher-Goldfarb-Shanno (BFGS) algorithm.[43–46] At each cycle, a Newton step is evaluated, which, by default, is constrained to lie within the quadratic region of the potential energy hyper-surface by a "trust radius" technique, as proposed by Simons and Nichols.[47] Convergence is checked on both gradient components and nuclear displacements.

B. The Internal-strain Tensor Approach

The elements of the force-response internal-strain tensor are second-energy derivatives with respect to an atomic displacement and to a lattice distortion:

$$\Lambda_{ai,v} = \left.\frac{\partial^2 E}{\partial u_{ai}\partial \eta_v}\right|_{\mathcal{E}} , \quad (7)$$

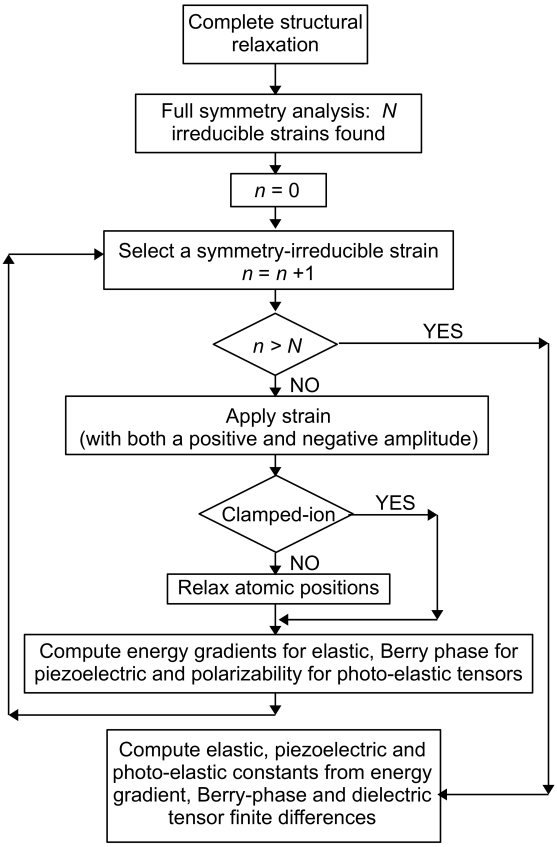

FIG. 1: Schematic flow-chart of the fully-automated algorithm implemented in the CRYSTAL program for the evaluation of second-order elastic constants via the geometry-optimizer approach for nuclear-relaxation contributions.

where u_{ai} are Cartesian components of the displacement vector $\mathbf{u}_a$ of atom a (i=x, y, z). A displacement-response internal-strain tensor $\mathbf{\Gamma}$, which describes first-order atomic displacements as induced by a first-order strain, can be defined as:[20]

$$\Gamma_{ai,v} = -\left.\frac{\partial u_{ai}}{\partial \eta_v}\right|_{\mathcal{E}} = \sum_{bj}(H^{-1})_{ai,bj}\Lambda_{bj,v} , \quad (8)$$

where $\mathbf{H}$ is the interatomic force-constant Hessian matrix of energy second derivatives with respect to pairs of periodicity-preserving atomic displacements:

$$H_{ai,bj} = \left.\frac{\partial^2 E}{\partial u_{ai}\partial u_{bj}}\right|_{\mathcal{E},\eta} . \quad (9)$$

When mass-weighted and diagonalized, the force-constant matrix of Eq. (9) provides vibration frequencies of Brillouin zone-center phonon modes. The $\mathbf{H}^{-1}$ matrix in Eq. (8) has to be considered a pseudoinverse of $\mathbf{H}$ where translational degrees of freedom are projected out, as discussed in detail elsewhere.[20]

The nuclear-relaxation contribution to elastic and piezoelectric constants can be expressed in terms of the

internal-strain tensor $\mathbf{\Lambda}$ (or $\mathbf{\Gamma}$):[20]

$$C_{vw}^{\rm nuc} = -\frac{1}{V_0}\sum_{ai}\Lambda_{ai,v}\Gamma_{ai,w}\ , \quad (10)$$

$$e_{kv}^{\rm nuc} = -\frac{1}{V_0}\sum_{ai}Z^*_{k,ai}\Gamma_{ai,v}\ , \quad (11)$$

where the $\mathbf{Z}^*$ tensor in Eq. (11) contains the Born dynamical effective charges:

$$Z^*_{k,ai} = \left.\frac{\partial^2 E}{\partial\mathcal{E}_k\partial u_{ai}}\right|_\eta . \quad (12)$$

In the current fully-automated implementation into the CRYSTAL program, the elements $\Lambda_{ai,v}$ of the force-response internal-strain tensor are here computed as finite differences of analytical lattice gradients with respect to atomic Cartesian displacements, by means of a generalized "Pulay's force method" originally proposed for interatomic force constants.[48] A double-sided finite difference formula has been implemented, according to which:[34]

$$\Lambda_{ai,v} = \left[g_v|_{\{u\}=0;u_{ai}=\overline{u}} - g_v|_{\{u\}=0;u_{ai}=-\overline{u}}\right]/2\overline{u}\ , \quad (13)$$

where $\overline{u}$ is the amplitude of the applied atomic displacement, with a default value of 0.003 Å. Use of a double-sided formula is generally preferable to a single-sided one as it allows for the cancellation of contaminating effects of cubic anharmonicity. When passing from the force-response $\mathbf{\Lambda}$ to the displacement-response $\mathbf{\Gamma}$ internal-strain tensor, the interatomic force-constant matrix $\mathbf{H}$ is required, whose calculation is also performed in a fully-automated fashion.[49] Given that the actual atomic Cartesian displacements to be considered for the SCF and analytical gradient calculation are the same for both objects, the current implementation for the internal-strain tensor has been devised in such a way to simultaneously compute $\mathbf{\Lambda}$ and $\mathbf{H}$, nearly at the same computational cost as for the calculation of $\mathbf{H}$ alone. The evaluation of $\mathbf{\Gamma}$ can thus be performed straightforwardly at the end of the calculation through the matrix multiplication in Eq. (8).

A schematic representation of the fully-automated algorithm (i.e. requiring a single run calculation) implemented in the CRYSTAL program for computing elastic constants via the internal-strain tensor approach is sketched in Figure 2.

The "internal-strain tensor" strategy is also implemented in the ABINIT package.

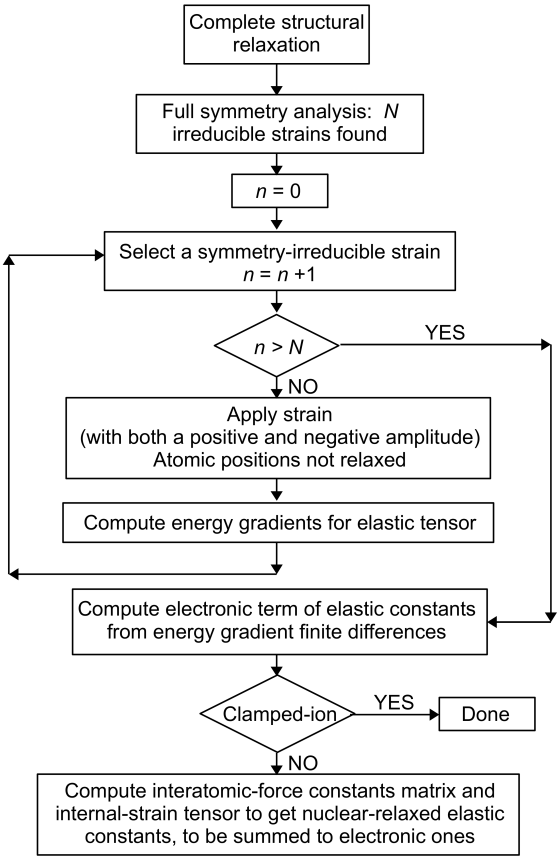

FIG. 2: Schematic flow-chart of the fully-automated algorithm implemented in the CRYSTAL program for the evaluation of second-order elastic constants via the internal-strain tensor approach for nuclear-relaxation contributions.

III. RESULTS AND DISCUSSION

The "geometry optimizer" and "internal-strain tensor" approaches to the determination of nuclear-relaxed elastic and piezoelectric constants of crystalline solids are here compared in terms of both numerical accuracy and computational performance. As recalled in Section II A, the "geometry optimizer" approach, despite being based on analytical energy gradients, is a complex procedure characterized by many numerical parameters and strategies (such as the particular choice of the Hessian guess, Hessian updating scheme, trust-radius scheme, convergence tolerances, etc.). On the contrary, the "internal-strain tensor" approach is a more analytical procedure, which requires the use and definition of just one numerical parameter (i.e. the atomic displacement amplitude $\overline{u}$) in the computation of the interatomic force-constant matrix $\mathbf{H}$ and of the force-response internal-strain tensor $\mathbf{\Lambda}$ from analytical gradient finite differences (see Eq. (13)). Such a parameter has been carefully optimized to the default value of 0.003 Å in the last decade.[34,49–51]

Two crystals are here considered, which have recently been used to test several numerical and computational aspects of different implementations of elastic and piezoelectric tensors: hexagonal zinc oxide (ZnO), which belongs to the $P6_3mc$ space group, and trigonal α-quartz, which belongs to the $P3_221$ space group.[31,34] All calculations have been performed with a developmental ver-

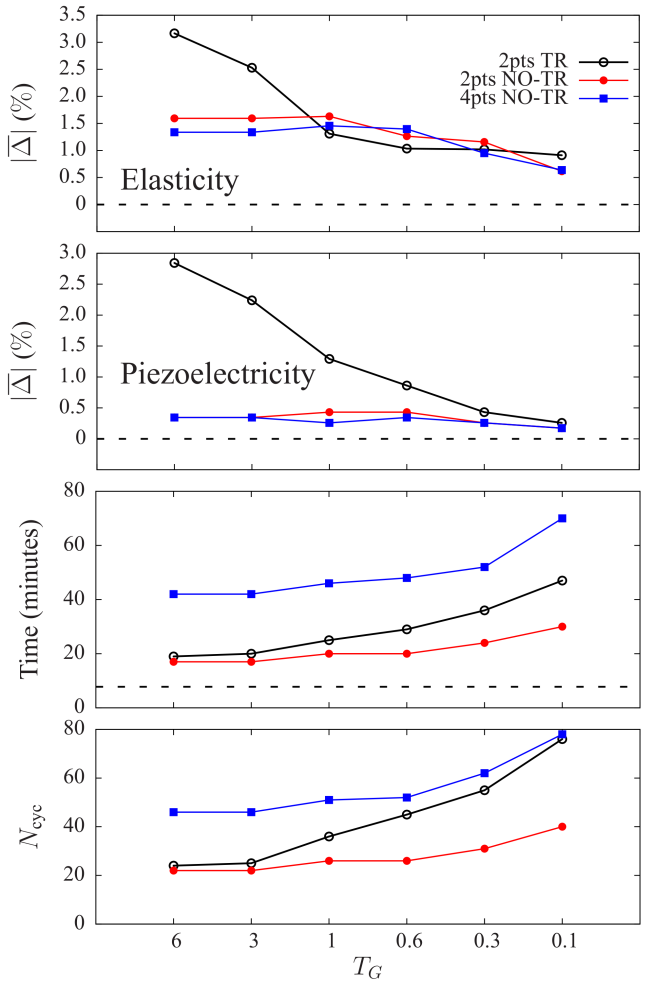

FIG. 3: (color online) For ZnO, mean absolute deviation $|\overline{\Delta}|$ (in %) of elastic (upper panel) and piezoelectric (second panel from the top) constants as computed within the "geometry optimizer" approach as a function of the optimizer convergence tolerance T_G with respect to elastic and piezoelectric constants obtained within the "internal strain tensor" approach. The time of the calculation, run in parallel mode over 16 processors, is given (in minutes) in the third panel from the top (the horizontal dashed line marks the time of the "internal strain tensor" calculation). The bottom panel reports the total number of required geometry optimization steps. T_G is in units of 10^{-4} a.u. The different lines correspond to different numerical settings, depending on whether use is made (TR) or not (NO-TR) of the trust-radius strategy and on the number of points used in the numerical finite differences of Eqs. (2) and (4).

sion of the CRYSTAL14 program,[52] by running in parallel mode over 16 Intel-Xeon processors working at 2.13 GHz, on a Linux cluster with Ethernet connection. The machine has 8 cores per node and 2 GB of memory per core. The PBE generalized-gradient exchange-correlation functional[53] is used in combination with all-electron basis sets of triple-zeta quality for all systems.[54]

The relative computational performance of the "geometry optimizer" approach with respect to the "internal-strain tensor" approach on the calculation of nuclear-relaxed elastic and piezoelectric constants of ZnO is documented in Figure 3. The IST approach is considered in its standard computational setup (see Eq. (13)). Several computational aspects of the GO approach are investigated as a function of the T_G threshold parameter, which is used to determine the convergence of the geometry optimization process based on the root mean square value of the gradients. This parameter is explored in the range 6×10^{-4} - 1×10^{-5} a.u.: the smaller this parameter, the tighter the convergence criterion. ZnO has 8 non-null elastic constants ($C_{11} \equiv C_{22}$, C_{33}, $C_{44} \equiv C_{55}$, C_{12} and $C_{13} \equiv C_{23}$) while the piezoelectric tensor is characterized by 5 non-null constants ($e_{15} \equiv e_{24}$, e_{33} and $e_{31} \equiv e_{32}$). In order to measure the deviation of nuclear-relaxed constants as obtained with the GO approach from IST ones, an overall index $|\overline{\Delta}|$ is introduced, which measures the mean absolute deviation (in %). For instance, for elastic constants, this index reads as:

$$|\overline{\Delta}| = \frac{1}{n} \sum_{vw} \frac{|C_{vw}^{\rm GO} - C_{vw}^{\rm IST}|}{|C_{vw}^{\rm IST}|} \times 100 \, , \qquad (14)$$

where the sum runs over the n non-null constants. An analogous index is defined for piezoelectric constants. These indices are reported in the two top panels of Figure 3, as a function of T_G. The black line corresponds to default settings in the GO approach (i.e. use of the "trust-radius" strategy and of 2 points in the numerical evaluation of the derivatives in Eqs. (1) and (3)), the red line corresponds to switching-off the "trust-radius" strategy and the blue line to switching-off the "trust-radius" strategy and using 4 points in the numerical evaluation of the derivatives. Some considerations: i) in all cases, as T_G becomes tighter, the mean absolute deviation $|\overline{\Delta}|$ decreases to values lower than 1% for elastic constants and 0.5% for piezoelectric constants; ii) the GO approach in its default computational conditions, with the "trust-radius" strategy on, shows a very slow improvement of the computed constants as a function of T_G (with mean absolute deviations of about 2.5% for both elastic and piezoelectric constants at the default value of $T_G = 3{\times}10^{-4}$ a.u.), with significant consequences on the corresponding computational cost of the calculation (to be discussed below); iii) switching off the "trust-radius" strategy makes the convergence with respect to T_G much faster (particularly so for piezoelectric constants); iv) use of 4 points instead of 2 in the numerical evaluation of the strain derivatives has a very little effect on computed constants.

The computational cost of the numerical GO approach with respect to the IST analytical one is documented in the third panel from the top in Figure 3, where the wall-clock time required for running the corresponding calculations, in parallel over 16 processors, is given (in minutes) as a function of T_G. The time needed by the analytical IST approach is represented by the horizontal dashed line. The computational cost of the GO approach

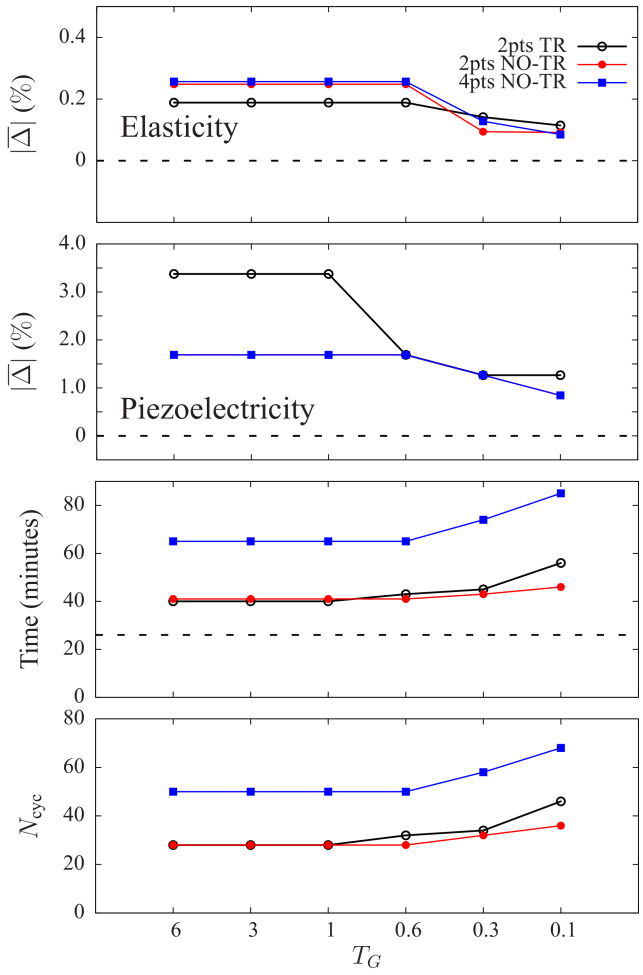

FIG. 4: (color online) For α-quartz, mean absolute deviation $|\overline{\Delta}|$ (in %) of elastic (upper panel) and piezoelectric (second panel from the top) constants as computed within the "geometry optimizer" approach as a function of the optimizer convergence tolerance T_G with respect to elastic and piezoelectric constants obtained within the "internal strain tensor" approach. The time of the calculation, run in parallel mode over 16 processors, is given (in minutes) in the third panel from the top (the horizontal dashed line marks the time of the "internal strain tensor" calculation). The bottom panel reports the total number of required geometry optimization steps. T_G is in units of 10^{-4} a.u. The different lines correspond to different numerical settings, depending on whether use is made (TR) or not (NO-TR) of the trust-radius strategy and on the number of points used in the numerical finite differences of Eqs. (2) and (4).

is obviously related to the number $N_{\rm cyc}$ of optimization steps, which is reported in the bottom panel of the figure. Some considerations on the computational performance: i) as T_G becomes tighter, the computational cost increases both in terms of required optimization steps and calculation time (particularly so when the "trust-radius" strategy is active); ii) as expected, the cost of the calculation doubles by using 4 instead of 2 points in the numerical evaluation of the strain derivatives; iii) remarkably, the cost (in terms of required time) of the IST calculation is always smaller than the GO one by a factor of about 2 at loose values of T_G, and of about 4 at tighter values of T_G.

Analogous considerations can be made as regards α-quartz, for which a comparison between the GO and IST approaches is presented in Figure 4, in terms of computational accuracy and performance. The structure of Figure 4 is the same as Figure 3. The α-quartz crystal is characterized by 11 non-null elastic constants ($C_{11} \equiv C_{22}$, C_{33}, $C_{44} \equiv C_{55}$, C_{12}, $C_{13} \equiv C_{23}$, and $C_{14} \equiv C_{56} \equiv -C_{24}$) and 5 non-null piezoelectric constants ($e_{14} \equiv -e_{25}$ and $e_{11} \equiv -e_{12} \equiv -e_{26}$). As regards the accuracy of the computed nuclear-relaxation term, the following considerations can be made: i) the two approaches provide almost the same values for the elastic constants, with a mean absolute deviation always smaller than 0.3%, which further reduces to about 0.1% at tight T_G values; ii) for piezoelectric constants, the mean absolute deviation becomes smaller than 1% but only for very tight values of T_G, whereas it is as large as 3.5% for less tight values of the convergence threshold when default settings of the GO approach are used, with the "trust radius" strategy active; iii) for piezoelectric constants, switching off the "trust radius" strategy makes the convergence with respect to T_G faster; iv) also in this case, as observed for ZnO, only slight changes in the computed constants are produced by using 4 points instead of 2 in the numerical evaluation of the strain derivatives.

Also in the case of α-quartz, the cost of the calculation of the nuclear-relaxation term of elastic and piezoelectric constants, in terms of required wall-clock time, is found to be smaller for the IST approach compared to the GO one, by a factor of about 2 at default T_G values and of about 3 at tighter T_G values.

Let us now discuss the relative computational performance of the GO and IST approaches to the calculation of the nuclear-relaxation term of the elastic tensor, as a function of the point-symmetry of the system. To do so, and to document the generality of the current implementation as well, we shall consider seven crystals belonging to the seven crystalline systems: diamond is taken as a representative of cubic lattices, which belongs to the F$d\overline{3}m$ space group and is characterized by 48 symmetry-operators in the corresponding point-symmetry group; zinc oxide is considered as a hexagonal crystal, which belongs to the P6_3mc space group with 12 point-symmetry operators; α-quartz represents trigonal lattices as it belongs to the P3_221 space group with 6 point-symmetry operators; the molecular crystal of urea has been chosen to represent tetragonal lattices, it belongs to the P$\overline{4}2_1m$ space group and it exhibits 8 point-symmetry operators; as a representative of the orthorhombic crystals, we consider one of the main constituents of the Earth upper mantle, α-forsterite, which belongs to the Pbnm space group with 8 point-symmetry operators; for the monoclinic crystalline system, a different polymorph of silica

TABLE I: For each of the seven crystalline systems, a representative crystal is chosen, whose main symmetry features are given in the table. The number of point-symmetry operators $N_{\rm sym}$, the total number of atoms per primitive cell $N_{\rm at}$ and the number of symmetry-irreducible atoms per primitive cell $N_{\rm at}^{\rm irr}$ are reported. The last four rows of the table report some indices related to the computational performance of the two alternative approaches for the evaluation of the nuclear-relaxation term of the elastic tensor: the "geometry optimizer" (GO) approach and the "internal-strain tensor" (IST) approach. The number of required SCF procedures plus analytical gradients calculations is given. The $|\overline{\Delta}|$ index (defined in Eq. (14)) gives the percentage mean absolute deviation of the nuclear-relaxation term of the elastic constants obtained with the two techniques (see text for details). The average absolute deviation $|\overline{\delta}| = 1/n \sum_{vw} |C_{vw}^{\rm GO} - C_{vw}^{\rm IST}|$ (in GPa) is also reported. Finally, for each system, the ratio between the time required by the GO calculation and that required by the IST calculation is reported.

Crystal	Diamond	Zinc Oxide	α-Quartz	Urea	α-Forsterite	Coesite	Albite
Formula	C	ZnO	SiO_2	$CO(NH_2)_2$	Mg_2SiO_4	SiO_2	$NaAlSi_3O_8$
Lattice	Cubic	Hexagonal	Trigonal	Tetragonal	Orthorhombic	Monoclinic	Triclinic
Space Group	F$d\overline{3}m$	P6_3mc	P3_221	P$\overline{4}2_1m$	Pbnm	C$2/c$	C$\overline{1}$
$N_{\rm sym}$	48	12	6	8	8	4	2
$N_{\rm at}$	2	4	9	16	28	24	26
$N_{\rm at}^{\rm irr}$	1	2	2	5	6	7	13
$N_{\rm SCF+G}^{\rm GO}$	6	22	28	160	97	98	160
$N_{\rm SCF+G}^{\rm IST}$	3	9	11	21	37	43	79
$|\overline{\Delta}|$ (%)	0.2	1.3	0.3	0.5	0.8	0.7	1.2
$|\overline{\delta}|$ (GPa)	0.004	0.8	0.2	0.4	0.2	0.2	0.1
$t^{\rm GO}/t^{\rm IST}$	2.0	2.6	1.6	3.1	1.6	0.8	0.8

is considered, coesite, which belongs to the C$2/c$ space group with 4 point-symmetry operators; finally, for triclinic lattices, low-albite has been chosen, which belongs to the C$\overline{1}$ space group and has 2 point-symmetry operators.

Selected symmetry features of these seven crystals are given in Table I, where the GO and IST approaches are also compared. The IST approach is considered in its standard formulation, Eq. (13), whereas the GO approach is used by switching off the "trust radius" strategy and by setting $T_G = 3{\times}10^{-4}$ a.u. The number of self-consistent-field (SCF) procedures plus analytical gradients calculation, $N_{\rm SCF+G}$, is reported for each system for both approaches. The mean absolute deviation $|\overline{\Delta}|$ (in %) between the nuclear-relaxed elastic constants evaluated with the GO and IST approaches, defined in Eq. (14), is also reported. For each system, the ratio $t^{\rm GO}/t^{\rm IST}$ between the time required by the GO calculation and that required by the IST calculation is reported in the last row of the table. Some considerations: i) in all cases, the two approaches provide very consistent sets of nuclear-relaxed elastic constants with the absolute mean deviation $|\overline{\delta}| = 1/n \sum_{vw} |C_{vw}^{\rm GO} - C_{vw}^{\rm IST}|$ always well below 1 GPa; ii) percentage mean deviations $|\overline{\Delta}|$ are below 1% in most cases (0.2% for diamond, 0.3% for α-quartz, 0.5% for urea, 0.7% for coesite and 0.8% for α-forsterite) and just slightly above 1% for the other two systems, 1.2% for albite and 1.3% for zinc oxide (note that in the case of albite the relatively high percentage deviation of 1.2% is only due to the existence of many tiny constants, given that the absolute mean deviation $|\overline{\delta}|$ is just of 0.1 GPa); iii) as we have documented before, the percentage mean deviation of 1.3% for zinc oxide would be reduced down to just 0.6% by further tightening the convergence threshold T_G (see Figure 3); iv) the number of SCF+G calculations required by the IST approach is always much smaller than that required by the GO approach (it has to be noted though that the typical residual symmetry in the SCF+G calculations in the GO approach is higher than that in the IST approach, which has a clear effect on timings); v) the IST approach is found to be faster roughly by about a factor of 2 (from 1.6 to 3.1) for crystalline systems from cubic to orthorhombic, whereas it is reported to be only slightly slower (by a factor of 1.2) for the monoclinic and triclinic systems.

IV. CONCLUSIONS

Two alternative computational approaches for the quantum-mechanical evaluation of the nuclear-relaxation contribution of elastic and piezoelectric coefficients of solids have been presented and discussed. A standard numerical approach based on geometry optimizations of atomic positions within strained lattice configurations has been compared in terms of both accuracy and computational efficiency to a quasi-analytical approach based on the evaluation of force-response internal-strain and atomic Hessian tensors.

The two approaches, as implemented in the public CRYSTAL program, are documented to provide very consistent sets of computed nuclear-relaxed elastic and piezoelectric coefficients when the "internal-strain tenor" approach is used in its standard formulation and very tight convergence criteria are used for the geometry optimization process, which, however, make the latter scheme significantly more costly in terms of computing time. In particular, the "geometry optimizer" approach is documented to suffer from a slow convergence of the results when a "trust radius" strategy is used for constraining the Newton step, which probably represents a too conservative procedure when significant deformations are applied to the lattice.

The "internal-strain tenor" approach has been documented to be more computationally efficient for most crystalline systems (cubic, hexagonal, trigonal, tetragonal and orthorhombic), whereas the "geometry optimizer" approach has been documented to be slightly more efficient for monoclinic and triclinic low-symmetry cases.

* Electronic address: alessandro.erba@unito.it

[1] R. D. King-Smith and D. Vanderbilt, Phys. Rev. B **47**, 1651 (1993).
[2] D. Vanderbilt, J. Phys. Chem. Solids **61**, 147 (2000).
[3] R. Resta, Rev. Mod. Phys. **66**, 899 (1994).
[4] A. Erba, K. E. El-Kelany, M. Ferrero, I. Baraille, and M. Rérat, Phys. Rev. B **88**, 035102 (2013).
[5] A. Mahmoud, A. Erba, K. E. El-Kelany, M. Rérat, and R. Orlando, Phys. Rev. B **89**, 045103 (2014).
[6] J. Baima, A. Erba, R. Orlando, M. Rérat, and R. Dovesi, J. Phys. Chem. C **117**, 12864 (2013).
[7] K. E. El-Kelany, P. Carbonnière, A. Erba, and M. Rérat, J. Phys. Chem. C **119**, 8966 (2015).
[8] K. E. El-Kelany, P. Carbonnière, A. Erba, J.-M. Sotiropoulos, and M. Rérat, J. Phys. Chem. C **120**, 7795 (2016).
[9] B. B. Karki, L. Stixrude, and R. M. Wentzcovitch, Rev. Geophys. **39**, 507 (2001).
[10] W. F. Perger, J. Criswell, B. Civalleri, and R. Dovesi, Comput. Phys. Commun. **180**, 1753 (2009).
[11] A. Erba, A. Mahmoud, R. Orlando, and R. Dovesi, Phys. Chem. Miner. **41**, 151 (2014).
[12] A. Zoroddu, F. Bernardini, P. Ruggerone, and V. Fiorentini, Phys. Rev. B **64**, 045208 (2001).
[13] R. Golesorkhtabar, P. Pavone, J. Spitaler, P. Puschnig, and C. Draxl, Comp. Phys. Commun. **184**, 1861 (2013).
[14] V. Milman and M. C. Warren, J. Phys.: Condens Matter **13**, 5585 (2001).
[15] D. Donadio, M. Bernasconi, and F. Tassone, Phys. Rev. B **68**, 134202 (2003).
[16] F. Detraux and X. Gonze, Phys. Rev. B **63**, 115118 (2001).
[17] A. Erba and R. Dovesi, Phys. Rev. B **88**, 045121 (2013).
[18] A. Erba, M. T. Ruggiero, T. M. Korter, and R. Dovesi, J. Chem. Phys. **143**, 144504 (2015).
[19] B. Mytsyk, A. Erba, N. Demyanyshyn, and A. Saharuk, Opt. Mater. (2016), in press.
[20] X. Wu, D. Vanderbilt, and D. R. Hamann, Phys. Rev. B **72**, 035105 (2005).
[21] M. Veithen, X. Gonze, and P. Ghosez, Phys. Rev. B **71**, 125107 (2005).
[22] R. Yu, J. Zhu, and H. Ye, Comp. Phys. Commun. **181**, 671 (2010).
[23] G. Saghi-Szabo, R. E. Cohen, and H. Krakauer, Phys. Rev. Lett. **80**, 4321 (1998).
[24] A. Dal Corso, M. Posternak, R. Resta, and A. Baldereschi, Phys. Rev. B **50**, 10715 (1994).
[25] M. Catti, Y. Noël, and R. Dovesi, J. Phys. Chem. Solids **64**, 2183 (2003).
[26] Y. Noël, M. Llunell, R. Orlando, Ph. D'Arco, and R. Dovesi, Phys. Rev. B **66**, 214107 (2002).
[27] M. Catti, Y. Noël, and R. Dovesi, J. Phys.: Condens. Matter **17**, 4833 (2005).
[28] K. Doll, R. Dovesi, and R. Orlando, Theor. Chem. Acc. **112**, 394 (2004).
[29] K. Doll, R. Dovesi, and R. Orlando, Theor. Chem. Acc. **115**, 354 (2006).
[30] A. Erba, M. Ferrabone, J. Baima, R. Orlando, M. Rérat, and R. Dovesi, J. Chem. Phys. **138**, 054906 (2013).
[31] J. Baima, A. Erba, L. Maschio, C. Zicovich-Wilson, R. Dovesi, and B. Kirtman, Z. Phys. Chem. **230**, 719 (2016).
[32] K. Doll, Molecular Physics **108**, 223 (2010).
[33] A. Erba, A. Mahmoud, D. Belmonte, and R. Dovesi, J. Chem. Phys. **140**, 124703 (2014).
[34] A. Erba, Phys. Chem. Chem. Phys. **18**, 13984 (2016).
[35] J. F. Nye, *Physical properties of crystals* (Oxford University Press, Oxford, 1957).
[36] M. Springborg, V. Tevekeliyska, and B. Kirtman, Phys. Rev. B **82**, 165442 (2010).
[37] M. Springborg and B. Kirtman, Theor. Chem. Acc. **130**, 687 (2011).
[38] I. Souza, J. Íñiguez, and D. Vanderbilt, Phys. Rev. Lett. **89**, 117602 (2002).
[39] B. Civalleri, Ph. D'Arco, R. Orlando, V. R. Saunders, and R. Dovesi, Chem. Phys. Lett. **348**, 131 (2001).
[40] K. Doll, Comput. Phys. Commun. **137**, 74 (2001).
[41] K. Doll, V. Saunders, and N. Harrison, Int. J. Quantum Chem. **82**, 1 (2001).
[42] H. B. Schlegel, Theoret. Chim. Acta **66**, 333 (1984).
[43] C. G. Broyden, IMA J. Appl. Math. **6**, 76 (1970).
[44] R. Fletcher, Comput. J. **13**, 317 (1970).

[45] D. Goldfarb, Mathematics of Computation **24**, 23 (1970).
[46] D. F. Shanno, Mathematics of Computation **24**, 647 (1970).
[47] J. Simons and J. Nichols, Int. J. Quantum Chem. **38**, 263 (1990).
[48] P. Pulay, Mol. Phys. **17**, 197 (1969).
[49] R. Dovesi, F. Pascale, and C. Zicovich-Wilson, in *Beyond Standard Quantum Chemistry: Applications from Gas to Condensed Phases*, edited by R. H. Lamoneda (Transworld Research Network, 2007), pp. 117–138.
[50] F. Pascale, C. M. Zicovich-Wilson, F. L. Gejo, B. Civalleri, R. Orlando, and R. Dovesi, J. Comp. Chem. **25**, 888 (2004).
[51] C. M. Zicovich-Wilson, F. Pascale, C. Roetti, V. R. Saunders, R. Orlando, and R. Dovesi, J. Comp. Chem. **25**, 1873 (2004).
[52] R. Dovesi, R. Orlando, A. Erba, C. M. Zicovich-Wilson, B. Civalleri, S. Casassa, L. Maschio, M. Ferrabone, M. De La Pierre, Ph. D'Arco, et al., Int. J. Quantum Chem. **114**, 1287 (2014).
[53] J. P. Perdew, K. Burke, and M. Ernzerhof, Phys. Rev. Lett. **77**, 3865 (1996).
[54] M. F. Peintinger, D. V. Oliveira, and T. Bredow, J. Comput. Chem. **34**, 451 (2013).